SUPPORTING INFORMATION

Quantitative and Comprehensive Decomposition of the Ion Atmosphere around Nucleic Acids

Yu Bai[†,‡], *Max Greenfeld*[§,‡], *Kevin Travers*[‡], *Vincent B. Chu*[¶], *Jan Lipfert*[**], *Sebastian Doniach*[¶,**,†], *Daniel Herschlag*[*,†,‡]

Biophysics Program and Departments of Biochemistry, Chemical Engineering, Applied Physics and Physics, Stanford University, Stanford, California 94305, USA

[*] Department of Biochemistry, Beckman Center B471, Stanford University, CA 94305, USA. Tel. 650 723-9442, FAX. 650 723-6783; Email: herschla@stanford.edu

[†] Biophysics Program

[‡] Department of Biochemistry

[§] Department of Chemical Engineering

[¶] Department of Applied Physics

[**] Department of Physics

We have developed a buffer equilibrium-atomic emission spectroscopy (BE-AES) approach to quantitate the ion atmosphere around nucleic acids (Fig. 2, Materials and Methods in the main text). In this Supporting Information, we describe the controls to determine the linear range and precision of the spectrometer (Table S1 and Fig. S1), to establish complete equilibration between the DNA-containing sample and the buffer (Fig. S3), and to validate the measurement of anion exclusion by cacodylate substitution (Fig. S4).

We also determined the competitive ion association with DNA duplexes of different sequence and length, and with a 24 bp DNA triplex (Scheme S1, Table S4 and Figs. S9, S10). The results are consistent with observations in the main text and support the conclusions described therein.

Spectrometer linear range and precision

The linear range and precision of the AES spectrometer for each element were determined as follows (Table S1). A concentration series of the element (μM-mM) was generated via sequential dilutions of a stock with known concentration (made with an absorption standard from SPEX CetriPrep (NJ); accuracy is within 2% in all cases). A comparison of the expected concentrations of the series versus the measured values establishes a "standard curve" for each element (Fig. S1).

The linear region of the standard curve is a concentration range within which the measured concentration (the mean plus/minus one standard deviation) falls within 5% of the expected value with an assumed linear dependence (Thermo Jarrell Ash, MA). The nonlinearities detected are consistent with the known instrument limitations [1]. The standard curve also provides empirical correction for data that extend into the non-linear regions.

The deviation in repeated standard curves gives the systematic precision of the spectrometer (Table S1 and Fig. S1). The standard curves for each element obtained in the absence or presence of the other elements were indistinguishable (within 5%, data not shown), indicating an absence of interference between the elements analyzed herein.

Equilibration between the DNA-containing sample and the buffer

In buffer equilibration (BE) (Fig. 2, step I in Materials and Methods), DNA (20-80 nmole) was diluted with 500 μL buffer and concentrated using Microcon YM-30 filters (Millipore, MA). The concentrated volume of the DNA-containing solution that retains in the top chamber of the filter is typically 100 μL, giving a final DNA concentration of 0.2-0.8 mM. This process is conducted in a 4^{o}C cold room.

We noticed that water evaporation can have a considerable perturbation on the ion concentration during the BE process. The bulk concentration of ion constituents in the DNA sample was monitored from the aliquot of flow-through (~50 μL) collected at the beginning, middle and end of the buffer exchange. At room temperature (25 ^{o}C), obtaining a final volume of 20 μL for the DNA sample in the top chamber led to a notable increase in the concentrations of all ion constituents (~15%, circles, Fig. S2A). Such a continuous change of the ion concentration rendered it difficult to assess the equilibration between the DNA sample and the indicated buffer. Additional control experiments strongly suggested that the water evaporation was responsible for the observed increase of ion concentrations as follows. YM-30 filters were set up in the same way as in the buffer equilibration (filter is pre-washed with 500 μL buffer to clear up the residual ions;

see also below), with 20 μL of buffer in the top chamber to mimic the concentrated volume of DNA-containing sample in BE. Leaving the filter at room temperature for the same time spent during buffer equilibration (~ 4 hrs) resulted in a similar increase in ion concentrations (10%, Fig. S2B, left most bars) as in the flow-through. Increasing the volume to 100 μL and lowering the temperature to 4 ^{o}C substantially suppresses the change (Fig. S2B, middle and right bars). Consistently, retaining a large volume in the top chamber and lowering temperature can eliminated significant evaporation and therefore have been used in the BE protocol (1-2% deviation with 100 μL retaining volume at 4^{o}C; diamonds, Fig. S2A).

With the above BE protocol, the equilibration between the DNA-containing sample and the buffer was examined by comparing the ion constituents in the flow-through to those in the buffer. In most cases, equilibrium was achieved after six or less rounds of dilution and concentration (Fig. S3A,B,D). For solution that contains very low divalent cations, eight rounds of buffer exchanges were performed (Fig. S3C).

Mock equilibration experiments with buffer solutions gave the same ion concentrations in the top chamber and in the flow-through, which were also the same as the starting solution (data not shown). This control demonstrated that residual ions in the filter prior and preferential binding of ions to the filter are insignificant.

Detecting anion exclusion by cacodylate substitution

To monitor the behavior of anions, as described in Materials and Methods in the main text, we substituted chloride ion with cacodylate ion [$AsO_2(CH_3)_2^-$], as the arsenic atom of cacodylate can be detected. Two critical controls were carried out to establish that cacodylate (pK_a 6.3) remains anionic in solution, such that its partitioning between the DNA-containing sample and the buffer reflects the behavior of the anion, and to ensure that there is no selective partitioning between chloride and cacodylate in the ion atmosphere.

The amount of excluded cacodylate is constant over the pH range of 7.4-8.5 for various ionic conditions (Fig. S4A), whereas a negative control in pH of 5.5 shows nearly zero exclusion of cacodylate, suggesting that cacodylate ions are fully deprotonated as anions in basic solutions. A pH of 8.0 was used for the DNA duplexes in this work. The stable formation of a pyrimidine-purine-pyrimidine triplex (*T24L*, Scheme S1) requires a pH of 5.1 so that no anion exclusion was measured for the triplex [2].

We next measured cacodylate exclusion in a DNA sample as a function of the fractional abundance of cacodylate ($\frac{[AsO_2(CH_3)_2^-]}{[M^-]}$, Fig. S4B) in various ionic solutions. The total anion concentration ($[M^-]$) was held fixed for each ionic condition. The amount of excluded cacodylate ion was linearly proportional to its fractional abundance and passed through zero for zero added cacodylate. We also confirmed that competitive cation association was not affected by the substitution of cacodylate ion for chloride ion (Fig. S4C). This observation suggests that the total excluded anions in the presence or absence of cacodylate is the same (according to charge neutrality of the overall system). Given the constant number of total excluded anions, the proportionality of cacodylate substitution is precisely what is expected for the case with no preferential exclusion of one anion relative to the other. For most ionic solutions studied in the text, sodium cacodylate was present at 80% of the total sodium salt.

The proportional dependence observed in Figure S4B allowed us to extrapolate from the observed amount cacodylate excluded ($AsO_2(CH_3)^-_{2depleted}$) at a given fractional abundance ($\frac{[AsO_2(CH_3)^-_2]}{[M^-]}$) to obtain the total number of excluded anion per DNA ($M^-_{depleted}$):

$$M^-_{depleted} = AsO_2(CH_3)^-_{2depleted} / \{\frac{[AsO_2(CH_3)^-_2]}{[M^-]}\} = AsO_2(CH_3)^-_{2depleted} \times \frac{[M^-]}{[AsO_2(CH_3)^-_2]} \quad \text{(S1)}$$

where $[M^-]$ and $[AsO_2(CH_3)^-_2]$ are the total anion concentration and the cacodylate concentration in the bulk, respectively. The total concentration of anions $[M^-]$ associated with the monovalent and divalent cations in the bulk, is calculated as $[M^+]+2\times[Mg^{2+}]$.

Determining the ion atmosphere from BE-AES measurements

Table S2 lists the ion counting results from a BE-AES experiment carried out with the 24 bp duplex (*24L*, Scheme S1) with varying concentrations of Na^+ and Mg^{2+}. The rows labeled "B" and "S" report the contents of the buffer solution and the sample containing DNA, respectively. There is, in general, excellent agreement between the stated bulk concentrations of Na^+ and Mg^{2+} and those determined for the buffer samples (±1-5%). DNA concentrations were determined directly by phosphorus measurements to minimize small variations in amounts from sample handling and pipetting error, thereby increasing the precision of the technique. The background amounts of phosphorus in the buffer and the background amounts of Mg^{2+} in samples with no added Mg^{2+} were within the random noise of AES measurements and are therefore neglected in calculating the ion excess (Eq. 1 in the main text).

The expectation for these data from first principles is that the system, DNA plus all ions, should be charge neutral. The final column of Table S2 shows that this prediction is met; in each case the overall charges of the DNA and its atmosphere sum to zero, within error.

The ion size effect is maintained under various ionic conditions

As stated in the main text, the relative affinity of cations with the same charge inversely correlates with ion size. Below we show that this order is determined by the ion identity rather than a specific experimental condition. We determined the relative association of the cations under a different background cation concentration (e.g., $[Na^+]$ is 10 mM in Fig. S5A vs. 50 mM in Fig. 4). Data in Figure S5A & B suggest an affinity order of $Li^+ > Na^+ > Rb^+$, the same as that obtained at 50 mM Na^+ (Fig. 4). In addition, the relative affinity of the cations was confirmed in binding competitions in which the competing and background cations were reversed (Fig. S5B).

An ion size effect is observed in competitions between monovalent and divalent cations

Figures S6 and S7 show the competitive association of monovalent cations (Li^+, K^+, Rb^+ and TMA^+) versus 5 mM Mg^{2+} and divalent cations (Ca^{2+}, Sr^{2+}, Ba^{2+} and putrescine^{2+}) versus 20 mM Na^+, respectively. In both cases, the inverse correlation of the ion competitiveness (*competition constant*) with the ion solvation radius is consistent with the observed ion size effect described in the main text (Fig. S8).

Interestingly, the alkali earth ions exhibit a smaller size effect in 20 mM Na^+ (Fig. S8B, 0.48-0.57 mM, 19% variation) than in 2 mM Mg^{2+} (Fig. 6B, 2.0-2.7 mM, 35%

variation). As noted in the main text, divalent cations are expected to be present at higher concentrations (relative to monovalent cations) near to the DNA, i.e., there is a more tightly bound ion atmosphere around the DNA. Thus, the competing divalent cations will experience more steric overlap with the more closely associated Mg^{2+} ions than the less closely associated Na^{+} ions, leading to greater size discrimination (see also the dependence of size effect on the thickness of the screening layer in ref. [3]. Indeed, an increased size effect is observed with increasing concentrations of background ions in size-Modified NLPB calculations and Grand Canonical Monte Carlo simulations (unpublished result from V. Chu and M. Engelhardt).

The ion size effect does not depend on DNA sequences

To examine whether the observed ion size effect is a property of the ion atmosphere or arises from the specific ion-DNA interactions, we conducted the same monovalent and divalent cation competitions as in Figs. 4 & 5, using DNA duplexes with alternate sequences (Scheme S1, $24L_{alt1}$, $24L_{alt2}$). These duplexes contain possible specific ion binding motifs such as A tracks ($24L_{alt1}$, $24L_{alt2}$) and GC rich sequences (from crystallized DNAs [4,5]). The competitiveness of ions is essentially identical regardless of the DNA sequence (Table S4), indicating that specific ion coordination, if any, is negligible in determining the association of the ion atmosphere with DNA.

The preferential association of divalent cations over monovalent cations is maintained with different DNA sequences and lengths

As shown in the main text, divalent cations are much more competitive than monovalent cations. The relative affinity of divalent cations is maintained for different DNA sequences, suggesting this preference is determined by the non-specific electrostatic interactions between the divalent cations and DNA (Table S4). The preferential association of divalent cations is also observed for 44 bp DNA duplex (*44L* in Scheme S1; Fig. S9C).

The competitiveness of divalent cations appears to increase with duplex length (the *competition constant* of Mg^{2+} in 20 mM Na^{+} is 0.48 and 0.37 mM for 24 and 44 bp duplexes, respectively, Table S4). This trend is also predicted by NLPB (0.95 and 0.79 mM, respectively, Table S4, and Figs. 7B & S9C). A physical interpretation of this effect is as follows. The presence of more phosphoryl groups of a longer duplex generates a stronger helical potential (note that electrostatic potential is long range), which enhances the attraction between DNA and the ions [6]. The increase of the attraction is proportional to ion valence according to Coulomb's law and thereby higher for divalent ions, resulting in a greater preference of the divalent ions in the atmosphere as duplex length is increased. This effect is expected to level off for duplexes beyond a certain length, and this critical length will depend on the ion environment [7,8].

Table S1: Linear range and precision of AES spectrometer

	Element									
	Li	**Na**	**K**	**Rb**	**Mg**	**Ca**	**Sr**	**Ba**	**P**	**As**
Linear dynamic range (mM) [a]	0.1-2.5	0.2-2.5	0.1-2.5	0.1-2.5	0.01-0.5	0.01-0.5	0.005-0.5	0.01-0.5	0.025-2	0.01-2
Deviation (%) [b]	1.3-1.0	2.2-0.9	2.2-1.5	1.1-0.5	0.8-1.0	1.3-0.7	2.6-0.6	1.7-0.3	1.5-0.8	2.7-1.0

[a] The concentration range of an indicated element within which the measured values that are bracketed by the standard deviation[b] depart no more than 5% from the expected values. Concentrations were measured in 4 mL sample.

[b] One standard deviation in multiple measurements. The deviation decreases as the element concentration increases because of improved signal-to-noise ratio. The values shown correspond to the boundaries of the linear range.

Table S2: Counting Na^+, Mg^{2+} and anion associated with *24L* (Scheme S1)

$[Na^+]$ (mM)[a]	$[Mg^{2+}]$ (mM)[a]	[DNA] (mM)[a]		$[Na^+]$ (mM)	$[Mg^{2+}]$ (mM)	$[AsO_2(CH_3)_2^-]$ (mM)	[DNA] (mM)	#Na^+ per DNA	#Mg^{2+} per DNA	#M^- per DNA[c]	Total charge[d]
20	0	0.2	B[b]	19.0±0.4	—	16.1±0.2	—	39.2±2.6	—	-6.3±0.6	-0.5±2.7
			S[b]	26.5±0.5	—	15.1±0.2	0.191±0.004				
20	0	0.4	B	20.4±0.4	—	17.0±0.2	0.003	39.8±1.9	—	-6.5±0.5	0.3±2.0
			S	33.3±0.7	—	15.3±0.2	0.325±0.006				
20	1	0.2	B	18.3±0.4	0.96±0.03	15.1±0.2	0.000	15.7±1.5	13.3± 0.6	-4.6± 0.9	1.0±1.9
			S	21.7±0.5	3.81±0.10	14.4 ±0.2	0.214±0.004				
20	1	0.5	B	22.4±0.4	0.99±0.03	16.5±0.2	0.001	16.6±1.3	13.7±0.6	-4.0±0.7	2.0±1.6
			S	31.4±0.6	8.38±0.25	14.9±0.2	0.539±0.01				
20	1	0.8	B	21.0±0.4	1.10±0.03	16.4± 0.2	0.001	15.2±1.3	13.8±0.4	-4.6±0.4	1.4±1.4
			S	33.6±0.7	12.5±0.04	13.7±0.2	0.825±0.02				

[a] The expected concentrations of cations and DNA. The total sodium salt (20 mM) is substituted by 16 mM sodium cacodylate (i.e., expected $[AsO_2(CH_3)_2^-]$ =16 mM).

[b] "B" and "S" stand for the buffer and the DNA-containing sample, respectively. Errors associated with measured concentrations correspond to the systematic precision of the AES spectrometer (Table S1 and Fig. S1). Standard error propagation was applied for the number of ions per DNA.

[c] Anion exclusion was determined by the cacodylate ($AsO_2(CH_3)_2^-$) substitution approach (Materials and Methods in the main text and Eq. S1).

[d] The total charge of the system is calculated as a sum over DNA charge, associated Na^+ and/or Mg^{2+}, and excluded anions: (-46) + (#Na per DNA) + (2 · #Mg^{2+} per DNA) – (# M^- per DNA).)

Table S3: The *competition constant* and apparent Hill coefficient ($[M]_{1/2}$ and *n* in Eq. 2, respectively) of monovalent and divalent competing counterions (CC) in binding to *24L* (Scheme S1). Association data of the background counterion (BC) in Figs. 4, 5, 7, 8, S6 & S7 are used to compute the values via Eq.2

BC											
50 mM Na^+			2 mM Mg^{2+}			5 mM Mg^{2+}			20 mM Na^+		
CC	**$[M]_{1/2}$ (mM)**	***n***	**CC**	**$[M]_{1/2}$ (mM)**	***n***	**CC**	**$[M]_{1/2}$ (mM)**	***n***	**CC**	**$[M]_{1/2}$ (mM)**	***n***
Li^+	35.9±0.6	1.09	Ca^{2+}	1.98±0.04	1.02	Li^+	65.3±1.8	1.27	Mg^{2+}	0.48±0.02	0.73
K^+	51.0±1.3	1.08	Sr^{2+}	2.50±0.07	0.99	Na^+	88.2±3.4	1.24	Ca^{2+}	0.49±0.03	0.68
Rb^+	57.5±2.1	1.07	Ba^{2+}	2.70±0.03	1.02	K^+	90.4±2.6	1.22	Sr^{2+}	0.55±0.02	0.67
NH_4^+	37.4±2.0	0.95	Put^{2+}	3.63±0.11	0.99	Rb^+	97.6±1.7	1.29	Ba^{2+}	0.57±0.01	0.65
TMA^+	77.7±2.1	0.99				TMA^+	120.0±5.0	1.14	Put^{2+}	0.84±0.10	0.59

Table S4: The *competition constant* (mM) of monovalent and divalent cations in associating with DNA duplexes of various sequence and length, and the DNA triplex (Scheme S1)

DNA	50 mM Na^+			2 mM Mg^{2+}			5 mM Mg^{2+}		20 mM Na^+	
	Li^+	**Rb^+**	**NLPB**	**Ca^{2+}**	**Sr^{2+}**	**NLPB**	**Na^+**	**NLPB**	**Mg^{2+}**	**NLPB**
24L	35.9±0.6	57.5±2.1		1.98±0.04	2.50±0.07		88.2±3.4	60	0.48±0.02	0.95
***24L*$_{alt1}$**	35.0±0.8	59.4±2.4		1.96±0.02	—		—	60	0.47±0.02	0.95
***24L*$_{alt2}$**	35.4±0.7	60.3±2.8	50	1.98±0.03	—	2	—	60	0.49±0.01	0.95
44L	34.8±0.6	59.0±1.1		—	2.56±0.07		—	63	0.37±0.02	0.79
T24L	35.7±1.3	60.1±2.0		—	2.60±0.05		111.4±2.8	71	0.25±0.01	0.73

Table S5: Radii of the hydrated monovalent and divalent cations

	Ion										
	Li^+	**Na^+**	**K^+**	**Rb^+**	**NH_4^+**	**TMA^+**	**Mg^{2+}**	**Ca^{2+}**	**Sr^{2+}**	**Ba^{2+}**	**Putrescine^{2+}**
Ionic radius [9]	0.60	0.95	1.33	1.48	—	—	0.65	0.99	1.13	1.35	—
First solvation shell [10, 11, 12]	2.2	2.5	2.8	3.0	2.9	4.5	2.1	2.4	2.7	2.9	—
Estimated radius [a]	3.6	3.9	4.2	4.4	4.3	5.9	3.5	3.8	4.1	4.3	5.3

[a] The radii of the hydrated monovalent ions and alkali earth ions are estimated as the distance from the ion to the water oxygen atom in the first solvation shell [10, 11, 12] plus an additional 1.4 Å for the water layer. The radius of putrescine^{2+} is crudely estimated as half of the average separation between N atoms (the closest: 3.3 Å, the furthest: 5.5 Å) plus the radius of an amine (1.65 Å) and a water layer (1.4 Å).

Scheme S1

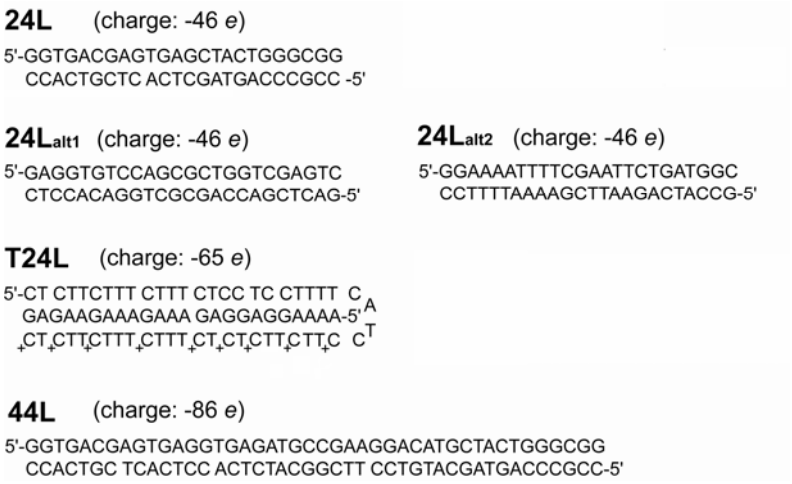
24L (charge: -46 e)
5'-GGTGACGAGTGAGCTACTGGGCGG
CCACTGCTC ACTCGATGACCCGCC -5'
24Lalt1 (charge: -46 e)
5'-GAGGTGTCCAGCGCTGGTCGAGTC
CTCCACAGGTCGCGACCAGCTCAG-5'
24Lalt2 (charge: -46 e)
5'-GGAAAATTTTCGAATTCTGATGGC
CCTTTTAAAAGCTTAAGACTACCG-5'
T24L (charge: -65 e)
5'-CT CTTCTTT CTTT CTCC TC CTTTT C
GAGAAGAAAGAAA GAGGAGGAAAA-5'
A
T
CT CTT CTTT CTTT CT CT CTT CTT C C
44L (charge: -86 e)
5'-GGTGACGAGTGAGGTGAGATGCCGAAGGACATGCTACTGGGCGG
CCACTGC TCACTCC ACTCTACGGCTT CCTGTACGATGACCCGCC-5'

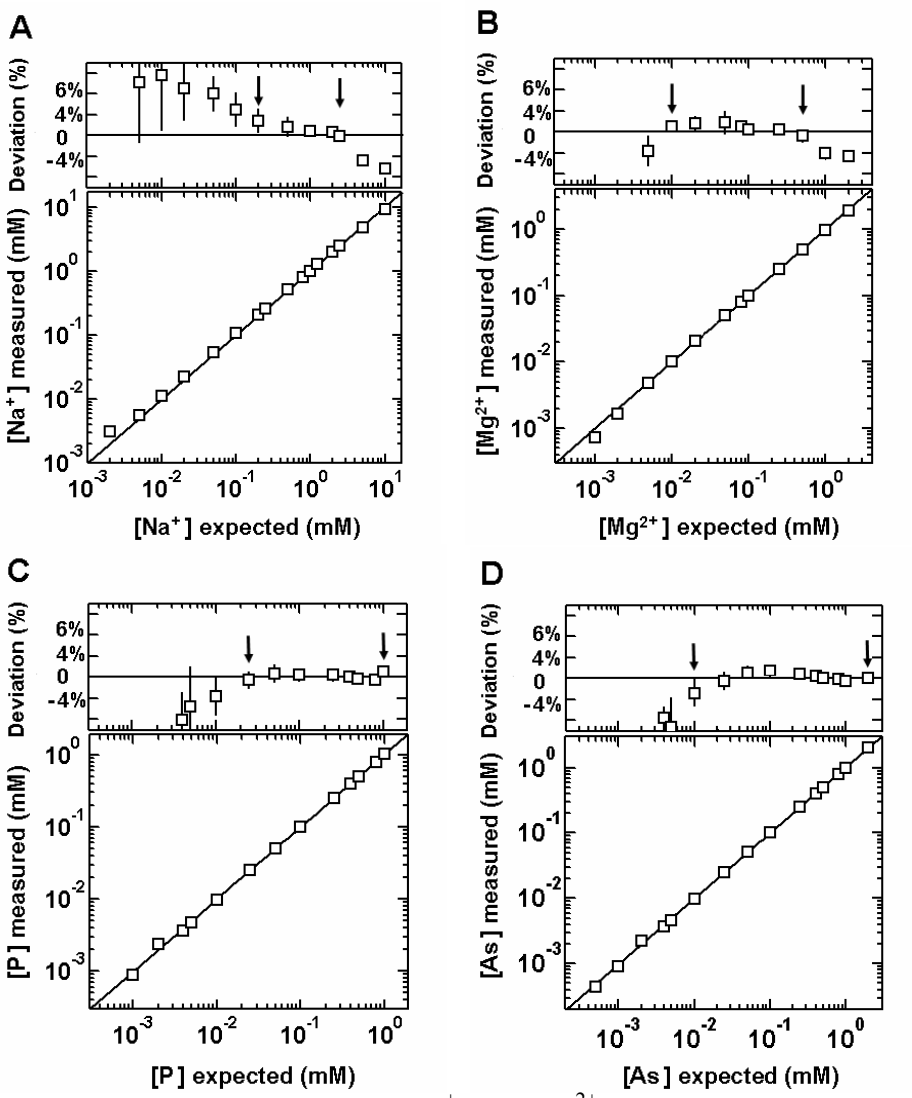

Figure S1: Standard curves of Na^+ (A), Mg^{2+} (B), phosphorus (C) and arsenic (D). The mean values of multiple measurements (greater than triplicates), in terms of the relative deviation from the expected values, are plotted above the main graphs (symbols are the same as in the main plots); the error bars represent the statistic error around the mean and are used to estimate the precision of the AES spectrometer (Table S1). Concentrations at which the measurement (a range of values bracketed by the error around the mean) departs less than 5% from the expectation are considered as within the linear range (arrows).

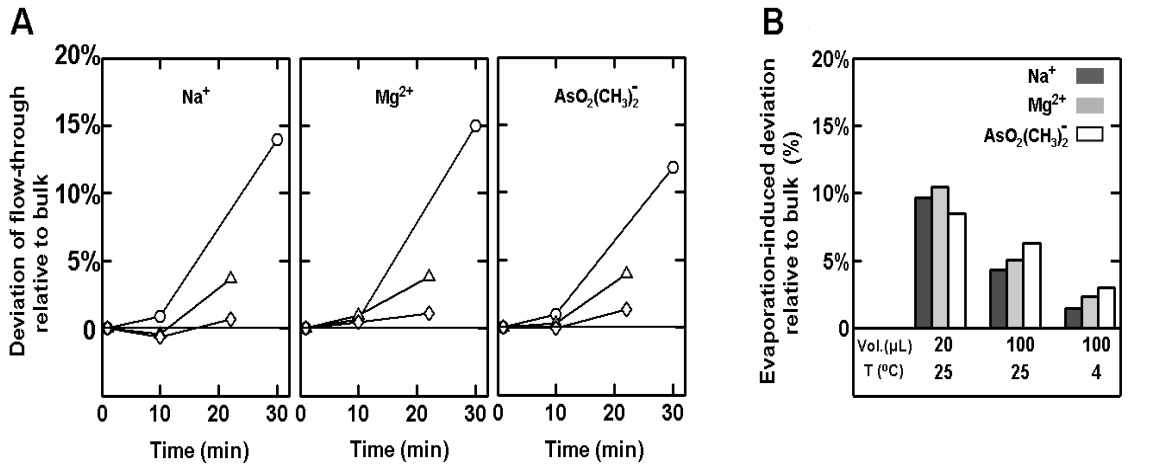

Figure S2: Perturbation of ion concentrations by water evaporation. A: Deviation of ion concentrations in the flow-through collected at 1, 10 and 20 or 30 minutes (corresponding to about 450, 250 and 100 or 20 μL solution retaining in the top chamber, respectively) during one round of the buffer equilibration (YM-30, spin at 3.0 rcf), relative to the starting solution (20 mM Na^+, 1 mM Mg^{2+}, 16 mM cacodylate). The buffer exchange was conducted at 25°C with a final volume of DNA sample of 20 μL (○), 25°C with a final 100 μL of DNA sample (Δ) and 4°C with a final 100 μL DNA sample (◊). DNA concentration has no significant influence on the magnitude of the deviations. The final volume of the filter-retaining sample and the working temperature are illustrated as in (A). B: Deviation of ion concentrations in the solution retained in the Microcon filters after 4 hrs, relative to the same starting solution above. Filters are set up as for the buffer equilibration procedure except no centrifuge spinning is applied. The retaining volume in the top chamber (Vol.) and the working temperature (T) are indicated.

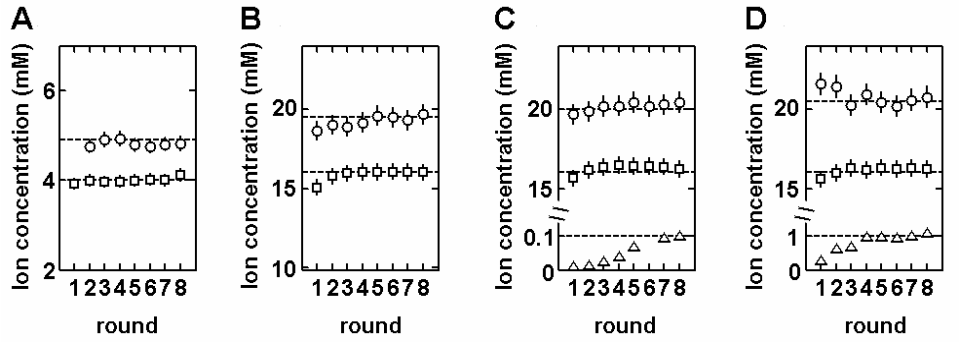

Figure S3: Equilibrium between the DNA-containing sample and the buffer is achieved by buffer equilibration. Plots show the ion constituents of the flow-through monitored after each round of buffer equilibration. A: 5 mM Na^+ total (○) and 4 mM cacodylate (□). B: 20 mM Na^+ total (○) and 16 mM cacodylate (□). C: 0.1 mM Mg^{2+} (Δ), 20 mM Na^+ total (○), and 16 cacodylate (□). D: 1 mM Mg^{2+} (Δ), 20 mM Na^+ total (○), and 16 cacodylate (□). 0.5 mM 24 bp DNA duplex (*24L*, Scheme S1) was used. With lower Mg^{2+} concentration (C), more rounds of buffer exchange are needed to reach equilibrium.

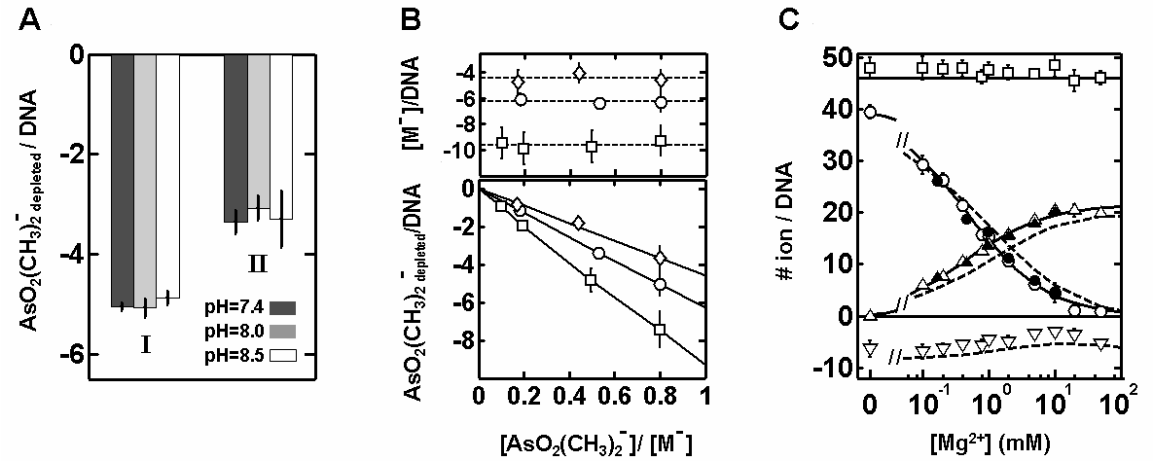

Figure S4: Measurement of the cacodylate exclusion at different pH values (A) and with different fractional abundances of cacodylate (B), and of the cation association in the presence and absence of cacodylate (C). A: The exclusion of cacodylate per DNA is constant in the range of pH tested (7.4-8.5, A) for various ionic solutions (I: 20 mM Na^+ with 10 mM cacodylate, II: 1 mM Mg^{2+} and 20 mM Na^+ with 10 mM cacodylate) indicating the dominant presence of the fully deprotonated, anionic cacodylate species. B: The observed cacodylate exclusion is plotted against the fractional abundance of cacodylate ($\frac{[AsO_2(CH_3)_2^-]}{[M^-]}$) in various ionic buffer: 20 mM Na^+ (○); 100 mM Na^+ (□); 20 mM Na^+ with 1 mM Mg^{2+} (◊). Lines are the least square fits for the data. The overall anion exclusion per DNA (Eq. S1) is plotted above the main graph (same symbols and x-axis as in the main plot). Values are consistent within error for each ionic solution (the average is indicated by a horizontal dashed line). C: Competitive association of Mg^{2+} vs. 20 mM Na^+ in the presence (Δ vs. ○) and absence (▲ vs. ●) of cacodylate. Data in the presence of cacodylate are taken from and plotted as in Fig. 7B (▽ for anion exclusion, □ for total charge). Dashed lines are NLPB predictions.

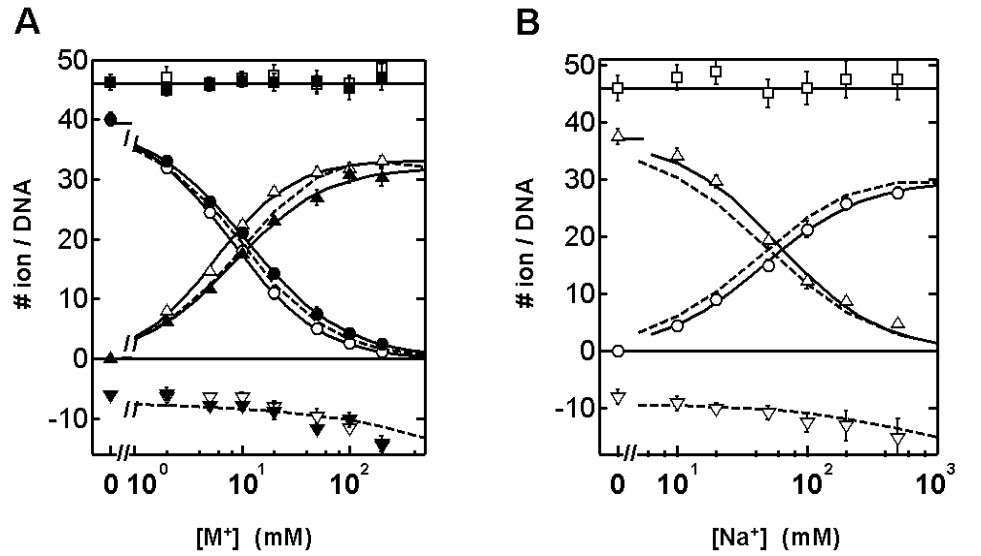

Figure S5: The competitive association of monovalent and/or divalent cations with the 24 bp DNA duplex (*24L*, Scheme S1). A: Li^+ (Δ) or Rb^+ (▲) vs. 10 mM Na^+ (○ or ●, respectively). B: Na^+ (○) vs. 50 mM Li^+ (Δ). The total charge of the ion atmosphere (□ and ■) is plotted as in Fig. 3 in the main text. Data are fit to Eq. 2 (solid curved lines) and compared to NLPB predictions (dashed lines).

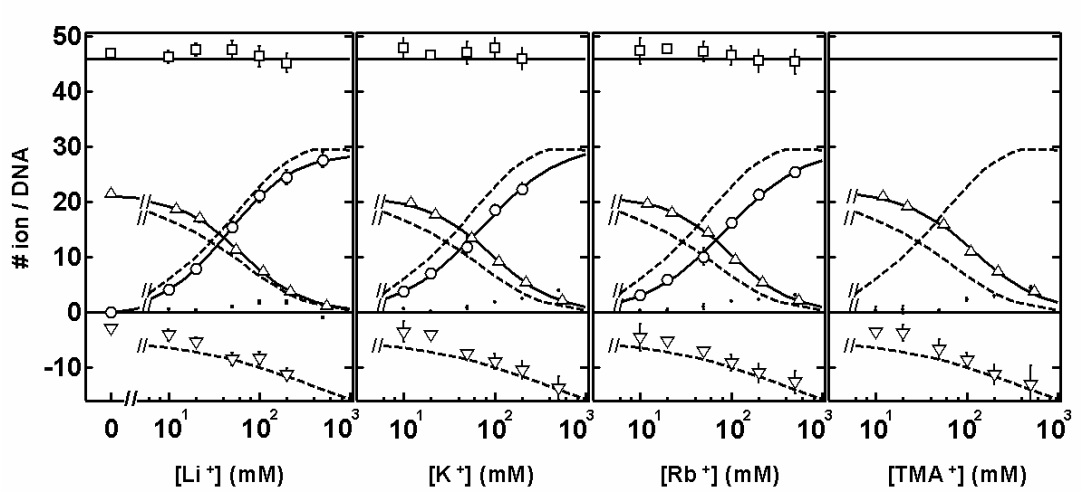

Figure S6: The competitive association of monovalent ions (○ for Li^+, K^+ and Rb^+; TMA^+ is not detectable by AES spectrometer applied in this work) against 5 mM Mg^{2+} (Δ) for the 24 bp DNA duplex (*24L*, Scheme S1). The total charge of the ion atmosphere (□) is plotted as in Fig. 3 in the main text. Data are fit to Eq. 2 (solid curved lines) and compared to NLPB predictions (dashed lines).

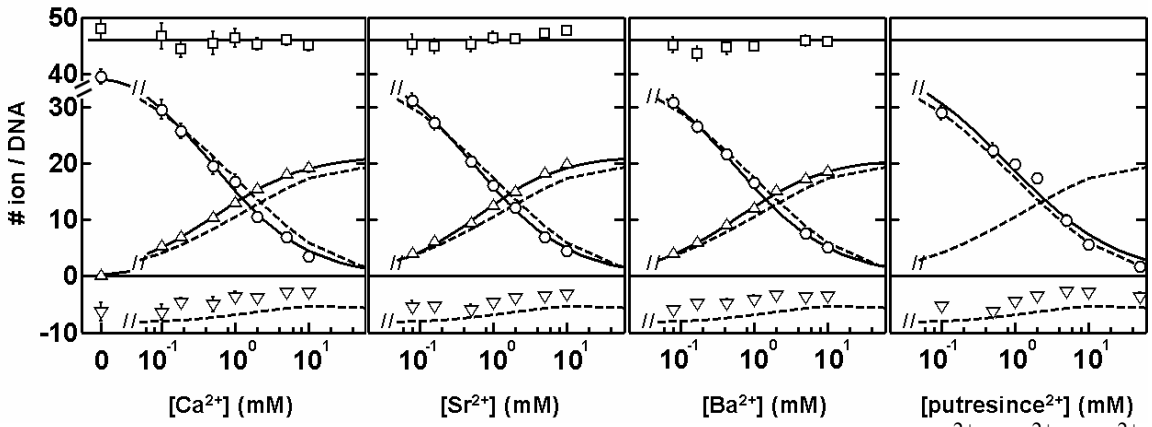

Figure S7: The competitive association of divalent ions (Δ for Ca^{2+}, Sr^{2+}, Ba^{2+}; putrescine^{2+} is not detectable by AES) against 20 mM Na^{+} (○) for the 24 bp DNA duplex (*24L*, Scheme S1). The total charge of the ion atmosphere (□) is plotted as in Fig. 3 in the main text. Data are fit to Eq. 2 (solid curved lines) and compared to NLPB predictions (dashed lines).

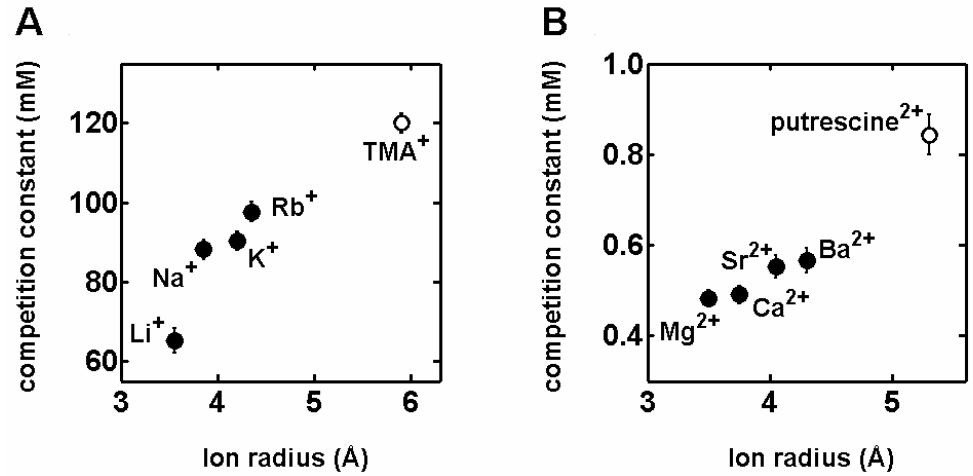

Figure S8: The inverse correlation between the affinity of monovalent cation (A) and divalent cation (B) and ion size. The *competition constants* are calculated for the series of monovalent cations competing against 5 mM background Mg^{2+} (A; data in Figs. 7A & S6) and for the series divalent cations against 20 mM background Na^{+} (B; Figs. 7B & S7) using Eq.2 . The radii of ions are the same as in Fig. 6.

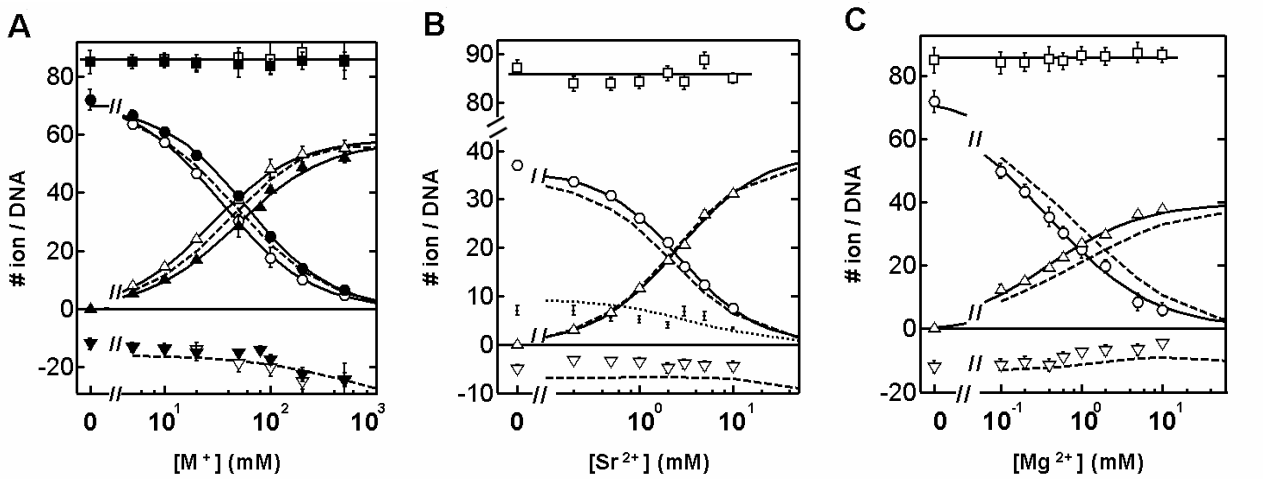

Figure S9: The competitive association of monovalent and divalent cations with a 44 bp DNA duplex (*44L*, Scheme S1). A: Li^+ (Δ) or Rb^+ (▲) against 50 mM Na^+ (○ or ●, respectively). B: Sr^{2+} (Δ) against 2 mM Mg^{2+} (○). C: Mg^{2+} (Δ) against 20 mM Na^+ (○). The total charge of the ion atmosphere (□ and ■) is plotted as in Fig. 3 in the main text. Data are fit by Eq. 2 (solid curved lines) and compared to NLPB predictions (dashed lines).

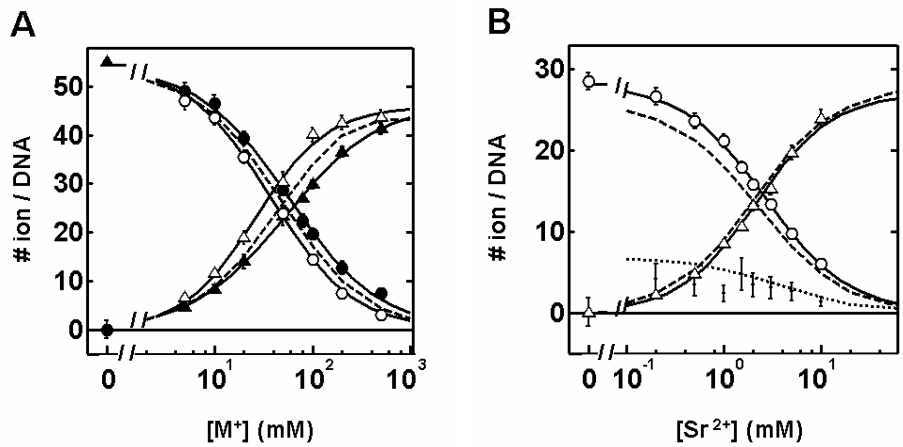

Figure S10: The competitive association of monovalent and divalent cations with the 24 bp DNA triplex (*T24L*, Scheme S1). A: Li^+ (Δ) or Rb^+ (▲) against 50 mM Na^+ (○ or ●, respectively). B: Sr^{2+} (Δ) against 2 mM Mg^{2+} (○). Data are fit by Eq. 2 (solid curved lines) and compared to NLPB predictions (dashed lines). Anion exclusion as well as the total charge of the ion atmosphere is not detected herein because an acidic solution (pH 5.1, below the cacodylate pK_a of 6.3) is required to stabilize the triplex.

Supporting References

(1) Chausseau, M.; Poussel, E.; Mermet, J. M. *Fresenius J Anal Chem* **2001**, *370*, 341-7.
(2) Shindo, H.; Torigoe, H.; Sarai, A. *Biochemistry* **1993**, *32*, 8963-9.
(3) Rouzina, I.; Bloomfield, V. A. *J Phys Chem* **1996**, *100*, 4305-13.
(4) Egli, M. *Chem Biol* **2002**, *9*, 277-86.
(5) Denisov, V. P.; Halle, B. *Proc Natl Acad Sci U S A* **2000**, *97*, 629-33.
(6) Tan, Z. J.; Chen, S. J. *J Chem Phys* **2005**, *122*, 44903 1-16.
(7) Olmsted, M. C.; Anderson, C. F.; Record, M. T., Jr. *Proc Natl Acad Sci U S A* **1989**, *86*, 7766-70.
(8) Olmsted, M. C. *J Biomol Struct Dyn* **1996**, *13*, 885-902.
(9) Shannon, R. D. *Acta Cryst* **1976**, *32*, 767.
(10) Ohtaki, H.; Radnal, T. *Chem Rev* **1993**, *93*, 1157-1204.
(11) Conway, B. E. *Ionic hydration in chemistry and biophysics* **1981**, Elsevier Scientific Pub. Co. Amsterdam.
(12) Garde, S., Hummer, G. & Paulaitis, M. E. *J Chem Phys* **1997**, *108*, 1552-61.